Cement and Concrete Research 177 (2024) 107414

Contents lists available at ScienceDirect

Cement and Concrete Research

journal homepage: www.elsevier.com/locate/cemconres

The neutralization of tricalcium aluminate hexahydrate and its spontaneous transformation into Friedel's salt, a layered double hydroxide

Eszter Kása [a], Yvette Szabó [a], Márton Szabados [a], Ákos Kukovecz [b], Zoltán Kónya [b], Pál Sipos [a], Bence Kutus [a,*]

[a] Department of Molecular and Analytical Chemistry, University of Szeged, Dóm tér 7–8, H–6720 Szeged, Hungary
[b] Department of Applied and Environmental Chemistry, University of Szeged, Rerrich Béla tér 1, H–6720 Szeged, Hungary

ARTICLE INFO

Keywords:
Tricalcium aluminate hexahydrate
Layered double hydroxide
Friedel's salt
Bayer process
Neutralization

ABSTRACT

Tricalcium aluminate hexahydrate, C_3AH_6, forms during the hydration of the oxide form, C_3A. Modelling the resulting phase composition over time has been the subject of intensive research; yet, understanding the effect of pH, a crucial parameter of cementitious mixtures, has remained elusive. To this end, we studied the stability of C_3AH_6 in a wide pH range via the addition of HCl. We compared the behavior of conventional 'cement' C_3AH_6 and 'Bayer' C_3AH_6, synthesized via alkaline digestion. Upon addition of HCl to mixtures in H_2O or NaCl, both phases slowly transform in an equilibrium reaction into Friedel's salt, $C_4ACl_2H_{10}$, a layered double hydroxide (LDH) with chloride ions being intercalated between the layers. Consequently, C_3AH_6, $C_4ACl_2H_{10}$, and $Al(OH)_3$ are likely to coexist in the pH range of 11–12. Furthermore, we find the reverse process, i.e. $C_4ACl_2H_{10} \rightarrow C_3AH_6$ to be kinetically hindered, consistent with the high stability of $C_4ACl_2H_{10}$ compared to hydroxide-intercalated LDHs.

1. Introduction

Cement production has reached an estimated 4.4 billion metric tons worldwide in 2021 [1]. The design of efficient and sustainable cementitious materials for the various purposes of construction industry requires detailed understanding of the behavior and physico-chemical properties of cementitious materials. The hydration of cement and the underlying solid-liquid reactions lie at the heart of cement chemistry, affecting setting time and hardening, the temporal evolution of pH and ion content of the liquid phase, the development of solid phases, etc. [2–8]. As an appreciation of the importance of hydration reactions, comprehensive thermodynamic models and databases have been published tabulating standard Gibbs energies or equivalent stability products of formation and dissolution for a large number of solid phases [2,9–15]. Thermodynamics, however, only applies if the reactions under consideration can progress without kinetic barrier, which is often not the case [16].

In this respect, the solid-state and aquatic chemistry of tricalcium aluminate, $Ca_3Al_2O_6$ or C_3A (where C = CaO, A = Al_2O_3 according to the conventional notation) is of particular interest, since it is the most reactive clinker phase upon hydration, amounting to 4–11 % of Portland cement [8,17–22]. C_3A is also present in alternative formulations, such as calcium sulfoaluminate [23–27] cements, proposed to be a 'greener' alternative to Portland cement due to its lower CO_2 emission, lower sintering temperature, better chemical resistance, faster setting, etc. [20,23–29]. However, a major drawback of calcium sulfoaluminate cements is their high production cost [20,24], primarily due to bauxite as the main alumina source. To tackle this problem, bauxite residue or red mud, which is the major by-product of the Bayer process, has been proposed to replace bauxite [30–34]. Using red mud, C_3A is introduced in its hydrated form, $Ca_3Al_2(OH)_6$ or C_3AH_6 (where H = H_2O, Fig. 1a), to the cement, since it forms in significant quantities during the so-called soda recovery step of the Bayer process [35,36].

A large body of research has been devoted to the analysis of the $C_3A \rightarrow C_3AH_6$ hydration reaction involving numerous intermediate solid phases forming, via studying either mixed clinker phases or neat C_3A. C_3A is known to transform into various layered double hydroxide (LDH) phases, e.g. C_2AH_8, C_4AH_{13}, and/or C_4AH_{19} [7,37–42], preceding the formation of katoite, C_3AH_6 [37–39,42–46]. The dissolution equilibria of C_3A as well as C_3AH_6 have been studied in detail, and corresponding thermodynamic solubility products for both solids have been determined [9,15,22,47].

* Corresponding author.
E-mail address: kutusb@chem.u-szeged.hu (B. Kutus).

https://doi.org/10.1016/j.cemconres.2023.107414
Received 10 August 2023; Received in revised form 14 December 2023; Accepted 18 December 2023

In equilibrium, other stable phases are either aluminum hydroxide, AH_3, or calcium hydroxide, CH, or LDH phases depending on the temperature and Ca:Al molar ratio [42,46]. Around room temperature, a phase boundary exists between C_3AH_6/C_4AH_{19} ($T < 19$ °C) and C_3AH_6/CH ($T > 19$ °C) aqueous systems at Ca:Al = 3:2 [42,48]. Moreover, C_4AH_{19} may exist in other hydration stages, i.e. C_4AH_{11} and C_4AH_{13}, respectively [7]. Further, these phases have a layered structure, consisting of $Ca_2Al(OH)_6^+$ layers as building blocks and various anions (OH^-, Cl^-, $Al(OH)_4^-$, NO_3^-, SO_4^{2-}, CO_3^{2-}) residing in the interlayer gallery to satisfy charge neutrality [7]. In particular, the chemical binding of external chloride is governed by the formation chloride-hydrocalumite or Friedel's salt, $Ca_4ACl_2H_{10}$ or $Ca_4[Al(OH)_6]_2Cl_2{\bullet}4H_2O$ (Fig. 1b), which is thus intimately related to the corrosion of reinforced concrete structures triggered by chloride ions [48–53]. Upon addition of CH to alkaline aluminate solutions in the absence of C_3A, the formation of C_3AH_6 can also take place in alkaline aluminate solutions via the association of Ca^{2+}, $Al(OH)_4^-$ and OH^- ions [54]. This reaction is rather slow, especially at room temperature, where CH and hydroxide-hydrocalumite, e.g. C_4AH_{11}, dominate the solid phase after 1 day.

In summary, the phase composition and solubility of calcium-aluminate phases are affected by temperature, Ca:Al molar ratio, and pH. However, the role of the latter in phase alterations upon hydration of cementitious materials has remained elusive, albeit it can vary in a wide range i.e. pH ≈ 12.5–13.7 (Portland cement) [2,5], pH ≈ 10.3–12.9 (calcium sulfoaluminate cement) [6], and pH ≈ 11.5–13.8 (concrete) [57]. For concrete, the pH can decrease even below 10 as a result of continuous leaching by water [58]. Equally important, C_3AH_6 may form under very different conditions, such as via hydration of C_3A [4,5,59,60] or alkaline digestion of CH in the Bayer process [35,61], which can alter the physico-chemical properties of these phases and hence may affect the mechanical properties of cementitious admixtures. Yet, such comparative study has not been published to the best of our knowledge.

To this end, we prepared C_3AH_6 via both hydrating C_3A and digesting CaO in hot sodium aluminate solutions and studied the response of their aqueous mixtures to changes in pH, both in water and NaCl solutions. We find these phases to be very similar in terms of their structure, crystallinity and morphology. In aqueous dispersions, the pH values reflect the solubility of C_3AH_6. Strikingly, upon addition of hydrochloric acid, we observe that C_3AH_6 transforms to Friedel's salt, which is the dominant solid phase between pH ≈ 10.2 and 11.5. In acidic medium, Friedel's salt dissolves yielding metal chlorides and mainly AH_3. Interestingly, in the presence of excess NaCl, the attainment of solubility equilibria is slower in the alkaline, but faster in the acidic regime.

2. Experimental

2.1. Synthesis of C_3AH_6

Irregular aluminum shots (99.9 %, Alfa Aesar) and NaOH solutions (from analytical research or a. r. grade NaOH pellets, VWR) were used to prepare a CO_2-free sodium aluminate stock solution with a composition typical to a Bayer "pregnant" or "green liquor", i.e. $[NaOH]_T = 7.5–8.0$ M (with a carbonate content of <0.1 mol%), and $[NaAl(OH)_4]_T = 4.6$ M, according to protocols published earlier [62,63]. (Hereafter, the subscript T denotes total or analytical concentration.) An equipment described previously [64] was implemented for the synthesis of Bayer C_3AH_6, modifying a procedure reported in [61]. Here, CaO made by calcining $Ca(OH)_2$ (97 %, VWR Chemicals) at 1000 °C for 8 h was added to the green liquor at a Ca:Al molar ratio of 1:1, and the mixture was stirred for 4 h in oil bath at $T \approx 95$ °C. The obtained product was washed with distilled water and dried under N_2 atmosphere using infrared lamp. As qualitative check for purity, the thus obtained product was calcined at 1300 °C for 4 h in a tube furnace; the X-ray diffractogram of the resulted C_3A matched with that of a literature reference (PDF #38–1429 [65]); see Fig. S1 in the Supporting Information, SI.

In addition, "cement" C_3AH_6 was synthesized with a well-known method, where CaO (made from calcining ≥99.0 % $CaCO_3$ at 1000 °C for 12 h) and Al_2O_3 (std. gr., Sigma-Aldrich) were used as starting materials in a $CaO:Al_2O_3 = 3:1$ M ratio [59]. The oxide was prepared by dry milling at 12 Hz for 30 min with a ball:sample mass ratio of 50:1 in a Retsch MM 400 mixer mill. (This pre-treatment in general increases the surface energy of solid particles via mechanical activation, which eventually leads to lower sintering temperatures.) After grinding, the solid was calcined at 1300 °C for 4 h. Using this method, a phase-pure product was obtained, and its reflection pattern agreed with that published earlier (PDF #38–1429 [65]), see Fig. S1, SI. The obtained oxide was hydrated (sample:water mass ratio of 1:5 or molar ratio of 1:60) for

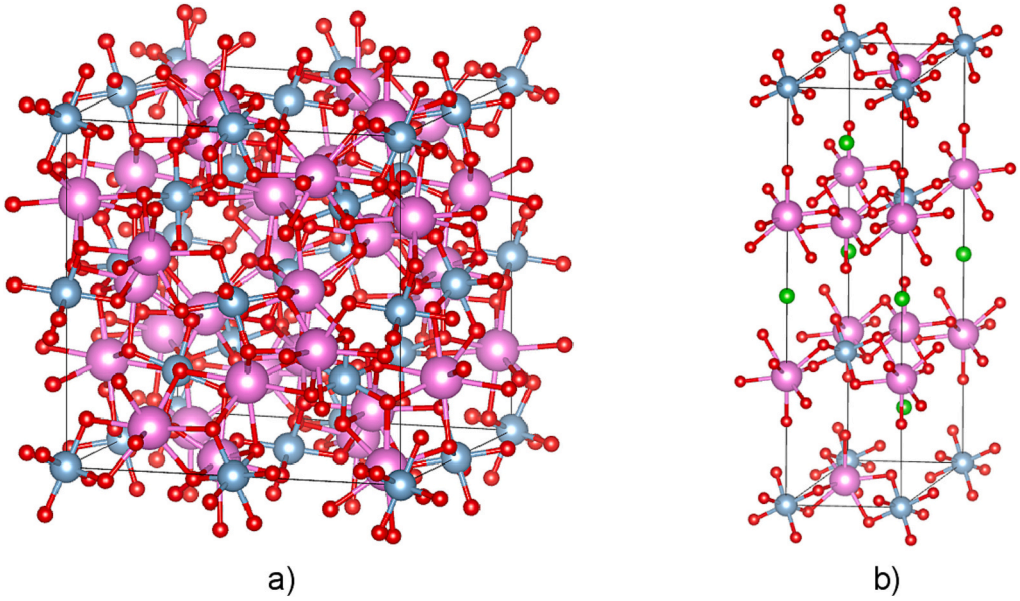

Fig. 1. Unit cell of a) C_3AH_6 (COD #1008157 [55]) and b) $Ca_4ACl_2H_{10}$ (Friedel's salt, ICSD #51890 [56]), with the following colour code for atoms: red (oxygen), silver-blue (aluminum), mauve (calcium), green (chlorine). For better visualization, hydrogen atoms are not shown. (For interpretation of the references to colour in this figure legend, the reader is referred to the web version of this article.)

two days at $T \approx 95$ °C in oil bath under N_2 atmosphere, followed by washing with distilled water and drying under N_2 atmosphere.

2.2. Elemental analysis

For both katoites, the Ca:Al molar ratio was determined with the aid of inductively coupled plasma mass spectrometry (type Agilent 7900). Here, 10 mg of solid was mixed with 100 mL water, then subsequent addition of 1 mL cc. HNO_3 (ICP-MS grade, VWR) lead to complete dissolution. For more accurate determination, both Sc(III) and Y(III) internal standards were added to the samples in a concentration of 100 ppb. The elemental ratios were determined to be 1.47 ± 0.04 for cement and 1.52 ± 0.03 for Bayer C_3AH_6 (based on three samples), which are in excellent agreement with the ideal 1.5:1 ratio.

Moreover, the Al(III) content was determined via classical gravimetric analysis for the Bayer solid. 2 g of sample was completely dissolved in ~64 mL 1 M HCl, then its tenfold diluted aliquot was used to precipitate Al(III) in the form of its oxinate (8-hydroxyquinolinate) complex in a 2 M CH_3COOH/CH_3COONH_4 medium at 70 °C. (99.8 % 8-hydroxyquinolin, a. r. grade glacial acetic acid and ammonium acetate, a.r. grade, were all purchased from VWR.) The Al(III) concentration derived from the weight of precipitate was only 1.1 % lower than the ideal one.

2.3. Structural characterization

The structural characterization of Bayer and cement C_3AH_6 as well as the phases forming from them were carried out by means of X-ray diffractometry (XRD), Fourier-transform infrared (FT-IR), ^{27}Al magic-angle-spinning (MAS) nuclear magnetic resonance (NMR) spectroscopy, N_2 adsorption-desorption BET, thermogravimetric analysis with mass spectrometric detection (TG/DTG-MS) and scanning electron microscopy with energy dispersive X-ray analysis (SEM-EDS), respectively. For detailed description of the instruments and measurement conditions, the Reader is referred to the SI.

2.4. Potentiometric titrations and batch measurements

First, separate samples were prepared for time-dependent (batch) measurements by suspending 2 g of solid in either 20 mL deionized water (Millex Synergy UV) or 20 mL 1 M NaCl solution (made from NaCl of a. r. grade from VWR Chemicals), thereby yielding an initial mass concentration of 100 g L^{-1}. In the next step, 21 mL of ~1.0 M HCl, in which the number moles of H^+ is equivalent to 4 OH^- ions of C_3AH_6 or $Ca_3Al_2(OH)_{12}$ (which will be referred to as 4 equivalents), was added to the suspensions under constant stirring. The stock solution of HCl was made by volumetric dilution of 37 wt% HCl (a. r. grade, VWR). The exact concentration of the titrant was determined via titrating a solution of dried $KHCO_3$ using methyl red as indicator. 20–120 min after acidification, the samples were filtered at different times, through 0.45 μm PTFE membrane filters using CO_2 traps. The filter cakes were collected and dried in N_2 atmosphere using infrared lamp. The dried solids were characterized via XRD, and selected samples were analyzed by TG-MS and EDS.

Furthermore, batch experiments were carried out to obtain information on the equilibrium pH and solid phases. Here, the initial compositions differed in the amount of added HCl (0–12 equiv. acid, i.e. 0–64 mL). Two series were prepared using either H_2O or 1 M NaCl solution as the dispersion medium, and the concentration of the solids was 100 g L^{-1} before the addition of HCl. After 1 day of mixing, the pH of the suspensions were measured using a Sentix H combined glass electrode (WTW), calibrated against buffer solutions. That is, solid-liquid contact was always established during pH readings. The suspensions were then filtered, dried, and measured via XRD, while the supernatants were analyzed for $[Al(III)]_T$ via gravimetry. All batch measurements were performed at (23 ± 2) °C.

To augment batch pH measurements, potentiometric titrations were carried out using a Metrohm Titrando 888 titration instrument equipped with a double-jacketed glass cell. First, suspensions of 100 g L^{-1} were stirred for one hour to allow equilibration, then a total volume of ~64 mL HCl, corresponding to 12 equivalents, was added stepwise to the mixture in 2 mL increments. A waiting time of 2 h was set between two aliquots. The cell potentials of the suspensions were measured by a calibrated pH electrode. Each solution was stirred continuously under N_2 atmosphere to prevent carbonation, while the temperature was kept at (25.0 ± 0.1) °C by a Julabo F12-MB thermostat.

3. Results and discussion

3.1. Characterization of katoites

It has been reported that the precursors of hydration can modify several properties of hydrogarnets, e.g. morphology, particle sizes, and even thermal stability [60]. Thus, the very different synthesis procedures for Bayer and cement C_3AH_6 require a comprehensive structural characterization of the as-prepared solids. Based on the powder X-ray diffractograms (Fig. 2a), there is no difference between the two tricalcium aluminate hydrates (JCPDS card no. PDF #24–0217 [65]), as both the positions and the relative intensities of the peaks are very similar. Moreover, the presence of an amorphous phase is discernible in the range of 10–40° 2θ, which is more pronounced for Bayer C_3AH_6. Given its maximum being at ca. 20°, this phase is probably amorphous AH_3. Nevertheless, the close agreement between the ideal katoite composition and the result of gravimetric determination indicate the contribution of this phase to be <2 wt%. In addition, we determined virtually the same mean size of ordered crystallites for the two solids (Table 1), considering the uncertainty of analysis. (To calculate these sizes, we took the average of the data for (420), (521), and (611) reflections, using the Scherrer equation with the shape factor being 0.9, based on fitting the entire diffractograms with a set of Lorentzians.) X-ray diffractograms for another lot of synthesized katoites are shown in Fig. S2a, SI. It has to be noted here that for the Bayer product, only the reflections of C_3AH_6 are seen. Conversely, the cement product exhibits the (001) and (002) reflections of monocarbonate-hydrocalumite, Ca_4AcH_{11} / $Ca_4[Al(OH)_6]_2CO_3 \bullet 5H_2O$ ($c = CO_3^{2-}$), (JCPDS card no. PDF #41–0219 [65]), suggesting that CO_2 was not completely excluded during the synthesis (as stock solutions of $NaOH/NaAl(OH)_4$ might contain <0.1 mol% Na_2CO_3), or it was adsorbed during the drying period. In general, this layered double hydroxide is a frequent by-product when hydrating calcium aluminates [60]. Based on the semi-quantitative approach described in Ref. [66], we estimate the amount of Ca_4AcH_{11} to be 8 ± 1 wt%, hence the lower limit of phase purity of C_3AH_6 is 92 wt%. Overall, we find the Bayer product to have a lower affinity for carbonation.

Likewise, the IR spectra (Fig. 2b; for another lot, see Fig. S2b, SI) further confirm the above findings, as all characteristic vibrations are found for both katoites with almost identical relative absorbances. We detect lattice OH stretching vibrations between 3000 and 3750 cm^{-1}, with a sharp one at ~3650 cm^{-1} and a broader one at ~3500 cm^{-1}, indicating water molecules situated in two different chemical environments. Also, noticeable amount of hydrating (surface) water molecules is apparent from the scissoring vibration mode at 1650 cm^{-1} in the case of cement C_3AH_6. Further, the signal at 790 cm^{-1} is the asymmetric stretching vibration of the M–O bonds. Moreover, signals of the surface adsorbed or interlayer carbonates from Ca_4AcH_{11} are also discernible around 1390 and 1510 cm^{-1}.

The thermogravimetric measurements of the katoites between 40 and 1000 °C are shown in Fig. 3a and b (for another synthesized products, see Figs. S3a and 3b, SI). Supporting the conclusions drawn from XRD and IR data, the thermal behavior of the samples is essentially the same. The DTG curves exhibit three endothermic transformations: the release of the physisorbed water or the dehydration of minor LDH/AFm phases [47,59] up to 150 °C, and that of the structural hydroxide groups

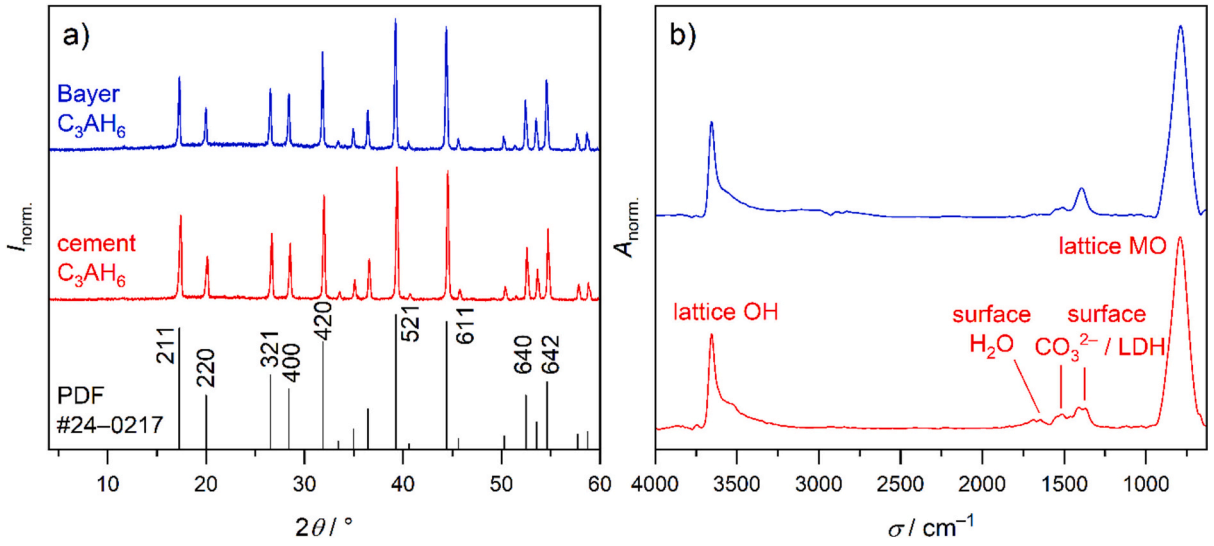

Fig. 2. a) Traces of powder XRD of the two tricalcium aluminate hydrates, i.e. cement (red) and Bayer (blue) C_3AH_6. The black diffractogram stands for literature reference (PDF #24–0217 [65]); shown are also the *hkl* indices of the most intense reflections. b) FT-IR spectra of the two C_3AH_6 phases (cement: red, Bayer: blue), with assignments of characteristic vibration bands. For panel b, LDH refers to a carbonate-containing layered double hydroxide, such as Ca_4AcH_{11} [7]. In both panels, measured data were normalized such that the highest value is unity. (For interpretation of the references to colour in this figure legend, the reader is referred to the web version of this article.)

Table 1
Physico-chemical attributes of the two tricalcium aluminate hydrates, i.e. cement and Bayer C_3AH_6: composition, surface area (SA), as well as the position (2θ), full width at half maximum (FWHM) of the three most intense reflections as obtained by fitting the powder diffractograms with a set of Lorentzians. The average crystallite sizes (D) were calculated from these data using the Scherrer equation.

C_3AH_6	Composition	SA / m^2 g^{-1}	2θ / °	FWHM / °	D / nm
cement	$3CaO•Al_2O_3•5.94H_2O$	1.7	31.97	0.176	46.5 ±
			39.38	0.182	0.3
			44.54	0.186	
Bayer	$3CaO•Al_2O_3•5.91H_2O$	1.4	31.83	0.160	49.0 ±
			39.23	0.176	1.8
			44.40	0.181	

up to 1000 °C, with the minimum being around 320 °C in the case of cement C_3AH_6 and 335 °C for Bayer C_3AH_6. Indeed, a loss at ~300 °C has been previously assigned to the dehydration of katoites [21,47,59]. A further loss at 440–460 °C indicates the respective water molecules to be in different environment, in agreement with the second OH band in the IR spectra. Moreover, although surface / LDH carbonate is detectable in the IR spectra, the corresponding departure of CO_2 would be expected well above 600 °C, see the discussion in Section 3.2.4. Overall, the total mass loss is 28.36 % (cement C_3AH_6) and 28.26 % (Bayer C_3AH_6), respectively. Since the theoretical maximum loss is 28.59 %, the solids contain 5.94 and 5.91 water molecules, respectively; see also Table 1. This small discrepancy is probably due to the presence of partially hydrated oxides or other minor phases, or slight loss of water upon drying. (For the other samples, these values are 5.76 and 5.90, see Fig. S3, SI.)

Regarding the textural attributes of the solids, the specific surface area of cement C_3AH_6 appears to be higher by ~20 % than that of the Bayer phase (Table 1); this difference is however comparable with

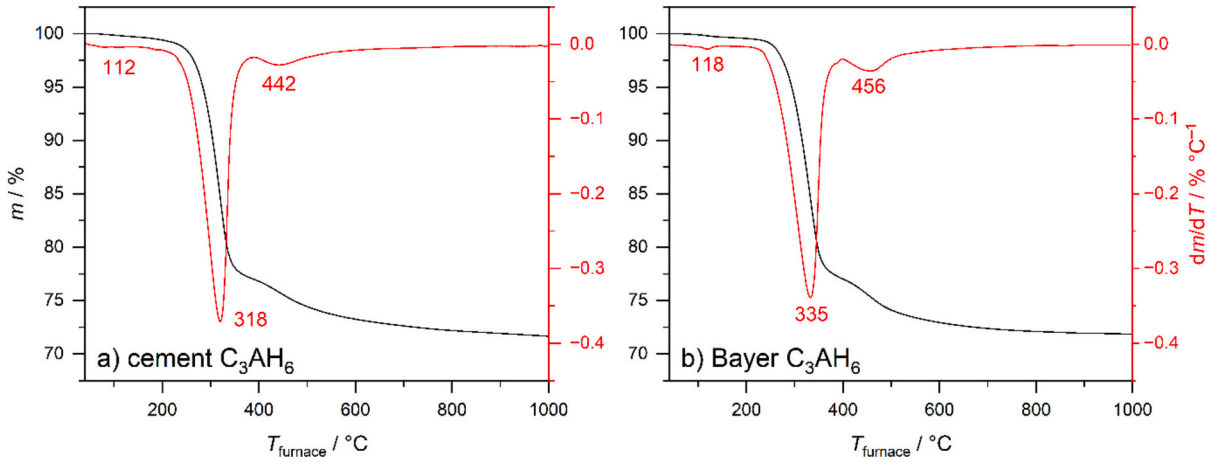

Fig. 3. Thermogravimetric analysis of the two tricalcium aluminate hydrates, i.e. cement (a) and Bayer C_3AH_6 (b). The left axis corresponds to the mass loss upon heating (black), while the right axis shows its derivative (red). Also shown are the characteristic losses, each corresponding to an inflection point on the TG curve. (For interpretation of the references to colour in this figure legend, the reader is referred to the web version of this article.)

uncertainty of data associated with the instrument used in this work. On the other hand, both phases have a ca. tenfold smaller surface area than the one reported earlier [67]. Such difference can be elucidated by the different average particle (or aggregate) sizes of the solids, as well as the choice of determination (e.g. Blaine vs. BET method [68]). The particle morphologies for the two katoites at three different magnifications are shown in Fig. 4a–e. Both solids are composed of irregular particle aggregates ranging from ca. 50 nm to 2 μm (Fig. 4b, c, e, f) which can from larger grains of 10 μm (Fig. 4a, c). For another lot of synthesized products, the micrographs are displayed in Figs. S4a-d, SI.

Further, we can infer on the coordination environment of the Al nuclei from the ^{27}Al MAS NMR measurements (Fig. S5, SI). In both cases, a symmetric signal is visible at 17.57 ppm with only a small (0–600 kHz) quadrupolar coupling constant. indicating octahedral coordination geometry [69].

3.2. The neutralization of katoites

3.2.1. Solubility of C_3AH_6 phases in water or 1 M NaCl solution

In the case of continuous titrations, we carried out five types of experiments by adding 1 M HCl to Bayer C_3AH_6 in H_2O (1), 0.3 NaCl (2), 0.5 M NaCl (3) or 1 M NaCl solutions (4), or to cement C_3AH_6 in 1 M NaCl solution (5). In each case, we allowed the suspensions to equilibrate for 1 h prior to the addition of the first aliquot of HCl. Furthermore, we performed batch titrations with the Bayer product in water (6) or 1 M NaCl solution (7), applying an equilibration time of 1 day. (We also made a repetition of (1), (5) and (6) to assess the reproducibility of the titrations.)

The thus obtained pH values, corresponding to the aqueous phases being contact with their solid phases, are 12.3 ± 0.3 (1), 12.0 (2), 12.7 (3), 11.9 (4), 12.3 ± 0.4 (5), 12.3 ± 0.3 (6) and 11.8 (7), respectively. All samples develop a strongly alkaline environment with an average pH of 12.2 due to the following dissolution reaction:

$$Ca_3Al_2(OH)_{12}(s) \rightleftharpoons 3Ca^{2+}(aq) + 2Al(OH)_4^-(aq) + 4OH^-(aq) \quad (1)$$

However, the pH values scatter around this average; therefore, no clear difference is seen between Bayer (4) and cement C_3AH_6 (5) phases, and no obvious trend is discernible for the Bayer katoite when increasing the concentration of NaCl. Nevertheless, it is apparent that the pH established after 1 h agrees well with that measured after 1 day, considering the uncertainty of pH determinations in these suspensions.

The dissolution reaction of cement C_3AH_6 has been studied earlier [12,15,46,59], described by the thermodynamic solubility product, log $K_{sp}(C_3AH_6)$, corresponding to infinite dilution:

$$K_{sp}(C_3AH_6) = \{Ca^{2+}\}^3\{Al(OH)_4^-\}^2\{OH^-\}^4 \approx [Ca^{2+}]^3[Al(OH)_4^-]^2[OH^-]^4 \Big/ (c^{\varnothing})^9 \quad (2)$$

where braces represent thermodynamic activities. In sufficiently dilute solutions, these quantities can be approximated with molar concentrations, shown as brackets ($c^{\varnothing}$ is 1 mol L^{-1} to ensure that $K_{sp}(C_3AH_6)$ remains dimensionless). To gain further information on the solubility of Bayer katoite, we determined the total concentration of aluminum(III), $[Al(III)]_T$, using gravimetry. The obtained concentrations are 0.0026 M in H_2O and 0.0014 M in 1 M NaCl with an average standard deviation of ±0.008 M. Since $[Al(III)]_T$ equals $[Al(OH)_4^-]_T$, these data allows us to estimate log $K_{sp}(C_3AH_6)$ to be −21.6 ± 1.2 (H_2O) and − 24.1 ± 1.2 (1 M NaCl) at room temperature. For water, our data agree broadly with log K_{sp} of −20.5 ± 0.2 and −20.4 ± 0.7 reported for cement C_3AH_6 [12,15,46,59], taking the associated uncertainty into account.

As for 1 M NaCl, the significantly lower log $K_{sp}(C_3AH_6)$ may reflect that our assumption of thermodynamic activities being equal to molarities (Eq. 1) does no longer hold at such high ionic strength [70]. Although log $K_{sp}(C_3AH_6)$ at 1 M NaCl is not available in the literature, it can be estimated by the Specific Ion Interaction Theory, SIT. SIT allows the estimation of activity coefficient γ_X, $\{X\} = \gamma_X[X]/c^{\varnothing}$, for component X, by introducing ion interaction parameters, ε, between the dissolved ions (Ca^{2+}, $Al(OH)_4^-$, OH^-) and those of the background electrolyte (Na^+, Cl^-). Following the methodology described in detail in Refs. [71,72], we calculate log $K_{sp}(C_3AH_6)$ to be −17.31 at 1 M NaCl. (For the calculations, the constant at zero ionic strength was taken as log K_{sp} of −20.5 [59]. Further, we used $\varepsilon(Ca^{2+},Cl^-) = 0.14$, $\varepsilon(OH^-,Na^+) = 0.04$, and we estimated $\varepsilon(Al(OH)_4^-,Na^+)$ with $\varepsilon(B(OH)_4^-,Na^+) = -0.07$; all values taken from Ref. [71].) This value contrasts our measured data of − 24.1, as it suggests an increase in solubility upon addition of NaCl, but

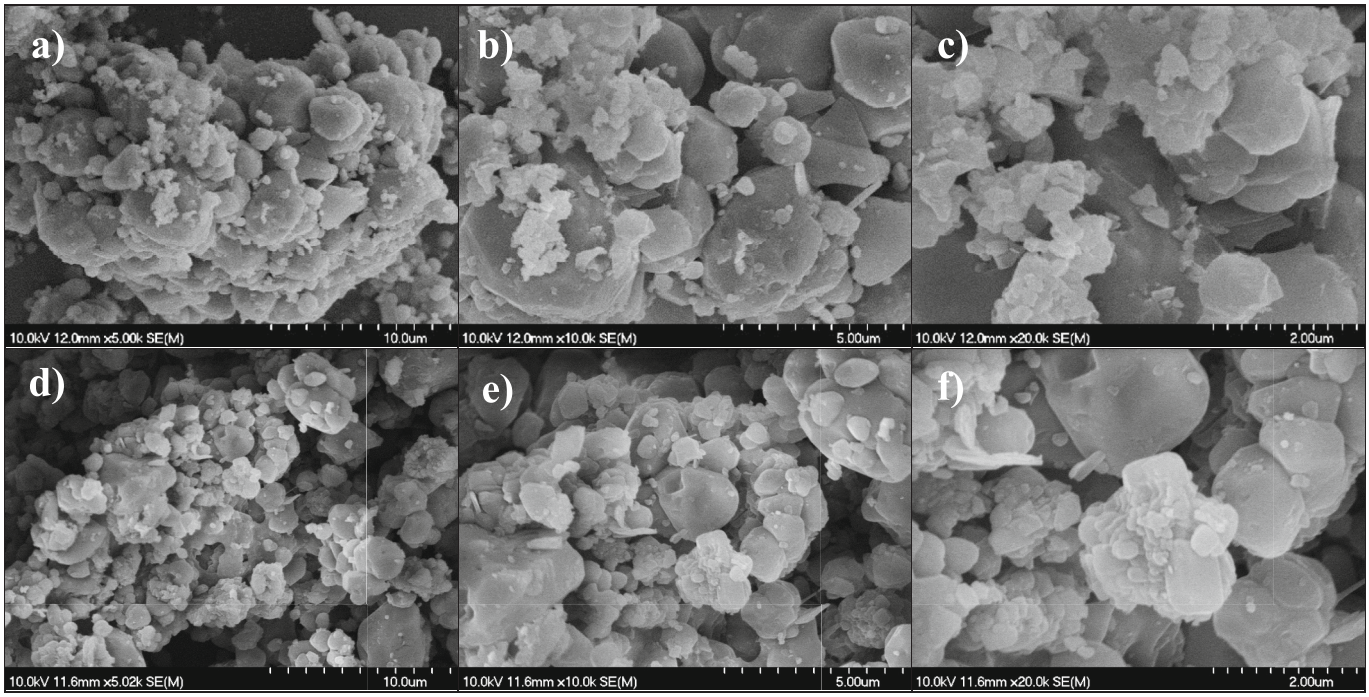

Fig. 4. Scanning electron micrographs of the two tricalcium aluminate hydrates, i.e. cement (a, b, c) and Bayer C_3AH_6 (d, e, f) at three different magnifications.

it agrees with the usually higher solubility of hydroxides at higher ionic strengths. Another explanation could be the more favorable precipitation of AH_3 in NaCl:

$$Al(OH)_4^-(aq) \rightleftharpoons Al(OH)_3(s) + OH^-(aq) \quad (3)$$

which would lower $[Al(III)]_T$ in the aqueous phase, thus the calculated log $K_{sp}(C_3AH_6)$. Indeed, we observe the peak of microcrystalline AH_3 at 18.1° in the diffractogram of the solid after 1 day of mixing (not shown), which can be assigned to the (002) reflection of gibbsite (PDF #70–2038) or bayerite (#83–2256) [65,69]. The equilibrium constant corresponding to Eq. (3), log $K(Al(OH)_4^-)$, can be obtained as log $K(Al(OH)_4^-) = -\log \beta(Al(OH)_4^-) - \log K_{sp}(AH_3)$, where the last two constants represent the stability product of the formation of $Al(OH)_4^-$ and the solubility product of gibbsite, respectively. Taking data from literature [70], we calculate log $K(Al(OH)_4^-)$ to be 1.13 (H_2O) as well as 0.83 (1 M NaCl), showing the precipitation of AH_3 to be actually less favorable in NaCl. Therefore, the lower $[Al(III)]_T$ possibly reflects that the gravimetric method we used is less reliable in concentrated salt solutions.

3.2.2. Time-dependent changes in the solid phase

We now turn to monitoring the time-dependence of the reaction between the two katoites and HCl. Here, we followed the temporal changes in the X-ray diffractograms for both solid phases for 2 h after the addition of 24 mL acid, equivalent to 4 OH^- ions of C_3AH_6. For Bayer C_3AH_6, Fig. 5a and b show the diffractograms at different apparent reaction times in H_2O or 1 M NaCl medium. (We note that filtration of the suspensions typically requires several minutes, thus, the real reaction time is somewhat longer than the stirring time, hence the term 'apparent'.) Based on the results of the 1-day batch measurements, the equilibrium pH in these systems is around 10.4.

As compared to the unreacted solid (stirred also for 2 h in each medium), we find new peaks to appear already 20 min after addition of HCl in water (Fig. 5a). These reflections show up at ~11.1°, 22.6°, 23.4°, 31.1°, 33.2, 38.7°, as well as two broad ones at ~18.3° and 20.5°. The latter two can be assigned to microcrystalline AH_3 [69], whereas the first group of peaks is indicative of LDH phases of hydrocalumite type with the general formula of C_4AXH_n, where the X^- interlayer anion can be SO_4^{2-}, CO_3^{2-}, OH^-, Cl^-, etc. Depending on the type of anion and water content, the interlayer distance may vary in the range of 8–12° 2θ [7,35,46,54,59]. In our series, chloride or hydroxide LDHs, or their mixtures are likely to form; we discuss the quantitative analysis of these solid phases in Section 3.2.4. Qualitatively, the same variations are observed also for cement C_3AH_6, as shown in Fig. S6, SI.

Surprisingly, the rate of LDH and AH_3 formation appears to be significantly lower in the case of 1 M NaCl as dispersion medium (Fig. 5b). These experiments are insufficient to disentangle the effect of NaCl, albeit a possible scenario can be envisaged based on an analogy with the dissolution of C_3A in the presence of gypsum and other sulfate salts [73–75]. It has been reported that C_3A dissolves incongruently in water, yielding an Al:Ca molar ratio of 2:1 instead of the ideal 3:2 one. Concurrently, the surface is enriched in Al(III), due to the precipitation of AH_3, which in turn adsorbs Ca^{2+} ions at the surface. In the presence of gypsum, the binding of SO_4^{2-} ions onto these positively charged spots can block active dissolution points, thereby slowing down the overall dissolution process. Similarly, the adsorption of Cl^- ions in concentrated NaCl media could reduce the dissolution of C_3AH_6, too. Since this dissolution is linked to the formation of LDH, the latter reaction would slow down, too.

3.2.3. The progress of neutralization in the entire pH range

We continue our analysis with monitoring the change in solution pH at different added acid equivalents, either in a form of potentiometric titrations or batch neutralization experiments. Fig. 6a and b show that regardless of the dispersion medium, the solid acts as a buffer in the pH range of 10–11. In this respect, the buffering capacity of red mud slurries in this region has been previously attributed to the dissolution of C_3AH_6 [47]. Interestingly, we find that the pH values obtained via titration for Bayer C_3AH_6 in H_2O (blue squares in Fig. 6a) agrees very well with the values obtained for separate solutions (i. e. batch pH measurements) for both H_2O and 1 M NaCl media (green and red squares in Fig. 6a). (Note that the incidental pH difference between the two media, which would arise from the different activity of H_3O^+ and from the change in the glass electrode's liquid junction potential, is around only 0.1 [76].) Since the batch pH values in both H_2O and 1 M NaCl were obtained in separate samples after 1 day of solid-liquid contact, it is reasonable to assume that these samples are close to thermodynamic equilibrium. Therefore, the data corresponding to titrations conducted in H_2O (blue squares) also represent equilibrium conditions.

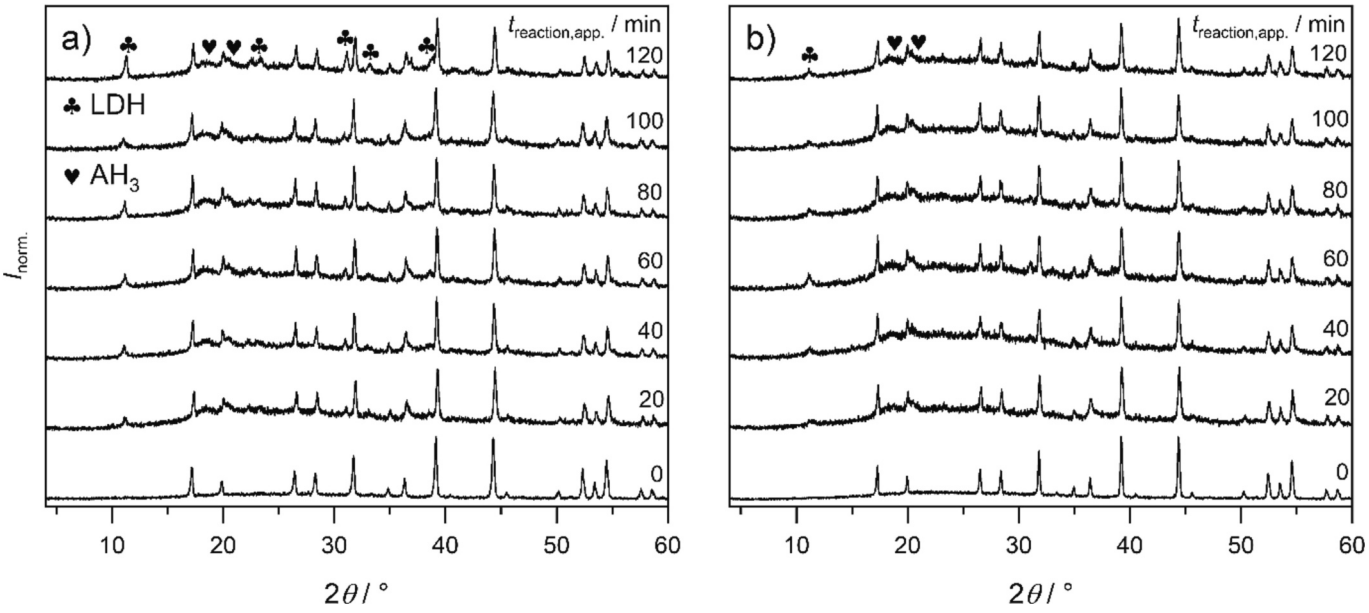

Fig. 5. Traces of powder XRD of Bayer C_3AH_6 at different apparent reaction times, $t_{reaction,app.}$, after addition of 4 equivalents of HCl to suspensions of 100 g L^{-1} in a) H_2O or b) 1 M NaCl. In both panels, the diffractogram at '0' minute stands for C_3AH_6 stirred for 2 h without acidification. Symbols show new phases forming upon neutralization, where $AH_3 = 2Al(OH)_3$ and LDH = layered double hydroxide. In both panels, measured data were normalized such that the highest value is unity.

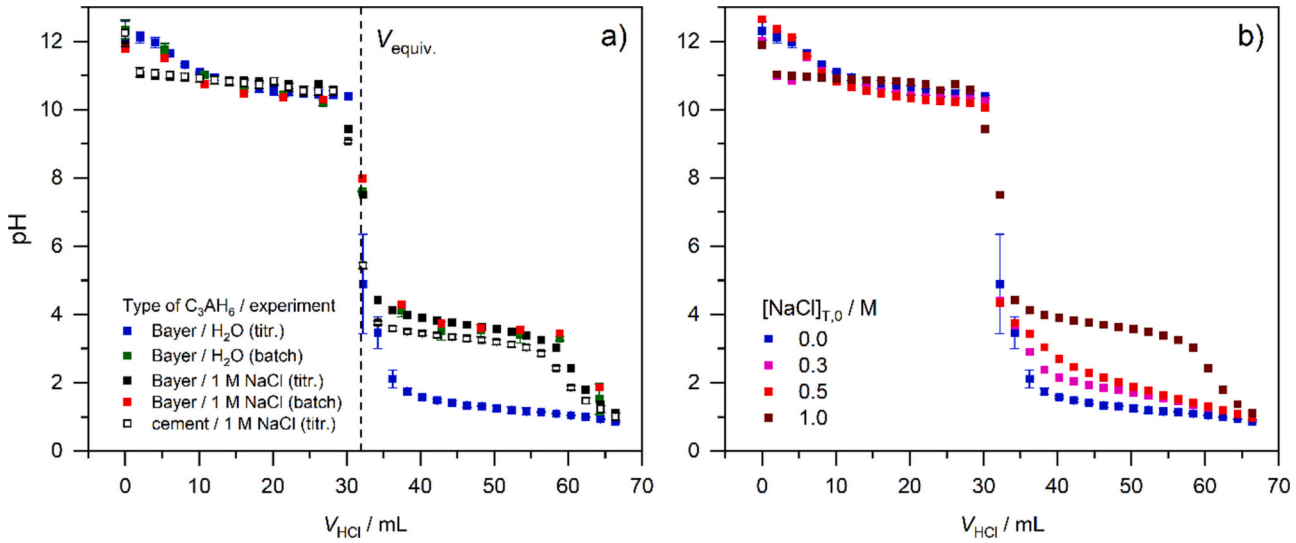

Fig. 6. Variation of pH as a function of added volume of HCl in suspensions of cement or Bayer C_3AH_6, measured via either potentiometric titrations or separate batch experiments. All pH readings were performed in the heterogeneous systems. The solids were suspended in H_2O or NaCl solution to have an initial mass concentration of 100 g L^{-1} and volume of 20 mL; the concentration of titrant HCl was 0.99 M. a) Comparison of cement and Bayer C_3AH_6 in H_2O (full blue and green squares) or 1 M NaCl (full and empty black, and full red squares). The vertical dashed line represents the calculated equivalence point, $V_{equiv.}$, corresponding to 6 equiv. HCl. b) Comparison of NaCl solutions (0-1 M) with different concentration for Bayer C_3AH_6. (For interpretation of the references to colour in this figure legend, the reader is referred to the web version of this article.)

As compared to these equilibrium data, the pH obtained by titrations in 1 M NaCl drops by ~1 already at $V_{HCl} = 2$ mL, reflecting the rapid neutralization of OH^- ions arising from katoite dissolution, and remains smaller up to $V_{HCl} \approx 10$ mL for both Bayer (black full squares) and cement C_3AH_6 (black empty squares). Consequently, the differences in pH between titrations conducted in H_2O together with batch measurements (blue, green and red squares) and titrations in 1 M NaCl (black full and empty squares) indicate that equilibrium has not yet been attained in the latter case. This apparent kinetic slowdown in NaCl is supported by the time-dependent powder X-ray diffractograms (Fig. 5), showing that the addition of 1 M NaCl decelerates the formation of the LDH phase (s). Possibly, the deceleration of kinetics arises from the blocking effect of Cl^- ions on the dissolution sites of C_3AH_6 [73–75]. To further explore the impact of NaCl on the titration curves, we also performed measurement at 0.3 and 0.5 M NaCl for the Bayer solid, shown together with data in H_2O and 1 M NaCl media in Fig. 6b. It is seen that the slowdown of reaction discussed above is noticeable only at 1 M NaCl.

Decreasing the pH further, an equivalence point ($V_{equiv.}$) shows up as in the case of classic acid-base titrations in the liquid phase; and its position is independent of the type of katoite or of the medium. Based on the initial mass concentration of the solids (100 g L^{-1}), the experimentally found $V_{equiv.}$ matches very well with the theoretical one (31.93 mL, shown as vertical dashed line in Fig. 6a), which corresponds to the consumption of 6 OH^- ions, i.e. 6 equivalents, for C_3AH_6. The reason of $V_{equiv.}$ being equal to the neutralization of 6 OH^- ions is that although C_3AH_6 dissolves progressively upon HCl addition, the Al^{3+} ions released into solution readily re-precipitate as AH_3 in the studied pH range due to the low solubility of gibbsite [70]. From an equilibrium point of view, this means that the three $Ca(OH)_2$ units of the katoites dissolve first, or in other words, they behave as 'strong base', whereas the AH_3 units dissolve only after this step, hence they can be regarded as 'weak base'. This is supported by the results of gravimetric measurements, where values of $[Al(III)]_T$ in the filtrates of the batch samples are at the limit of detection or could not even be determined in the alkaline range, while it increases steeply above 6 equiv. HCl (Fig. S7, SI). The overall process is summarized by the following equation:

$$Ca_3Al_2(OH)_{12}(s) + 6HCl(aq) \rightarrow 3CaCl_2(aq) + 2Al(OH)_3(s) + 6H_2O(aq) \quad (4)$$

In the acidic pH region, we find the pH values for Bayer C_3AH_6 in H_2O (blue squares, Fig. 6a) are significantly smaller (by 2–2.3 pH units) than the batch values (red and green squares), the latter data again representing equilibrium conditions. Based on the discussion on the alkaline regime, H_2O appears to slowdown the dissolution kinetics of the forming AH_3. Conversely, titration data for 1 M NaCl (full black squares) agree well with the batch values; thus, the addition of salt helps attain chemical equilibrium at a faster rate as compared to H_2O. The latter observation is supported by titrations at different salt concentrations: as the concentration of NaCl increases (0 → 1 M), equilibrium is reached proportionally faster, shown in Fig. 6b.

This notion is the opposite of what we found in the alkaline regime, where NaCl had a decelerating, and H_2O had an accelerating effect on dissolution rates. Here, such reversal of the medium effect on kinetics upon entering in the acidic range suggests the underlying mechanism to be very different. Previously, the dissolution of gibbsite has been found to be actually slowed down in 0.02 M NaCl as compared to water [77], as a result of negative kinetic salt effect based on the Debye-Hückel theory [78]. Further, studying different salts suggested the role of anions to be crucial for the reduction of dynamics. On the other hand, an increase in the dissolution kinetics has been observed for calcite at 0.1 M NaCl [79], which falls beyond the validity of the Debye-Hückel equation, where specific ion effects (e.g. hydration) come into play. Also, surface ion pairing between Al^{3+} and Cl^- ions promoted by the high concentrations of Cl^- ions in the bulk may enhance the rate of dissolution. Overall, our observations suggest the faster dissolution found for calcite in concentrated electrolytes to be also relevant for the dissolution of AH_3 in 1 M NaCl.

Another difference between the titration curves is seen when comparing Bayer (black full squares) and cement C_3AH_6 suspensions in 1 M NaCl (black empty squares), since the latter yield markedly lower pH values (by ca. 0.5, see Fig. 6a), indicating again that the latter solid attains solubility equilibrium slower. Since the two solids behave identically before the equivalence point, this difference can be attributed to morphological differences in the forming AH_3. Possibly, cement C_3AH_6 transforms into gibbsite of higher crystallite size, which is known to decrease the solubility in the case of goethite, FeOOH [80].

We also analyzed the solid phases obtained for Bayer C_3AH_6 batch samples in H_2O or 1 M NaCl at each added HCl equivalent. (That is, each solid phase corresponds to the supernatant pH values indicated by green

or red squares in Fig. 6a). We find that upon acid addition, salient variations take place in the solid phase in both media, as demonstrated by the powder diffractograms corresponding in Fig. 7a and b. First, untreated Bayer C_3AH_6 stirred in H_2O for 1 day exhibits a small-intensity peak at 11.9° (Fig. 7a, inset), which belongs to an LDH phase, either monocarbonate-hydrocalumite, Ca_4AcH_{11}, or hydroxide-hydrocalumite, Ca_4AH_{11} [7,35,46,54,59]. (It is worth mentioning that the primary phases present in heterogeneous systems are usually C_4AH_{13} or C_4AH_{19}, which however undergo dehydration when drying the solids [7,59].) Ca_4AcH_{11} could form via the absorption of aerial CO_2 by the suspension during filtration or drying. On the contrary, C_4AH_{11} could form as a hydrolysis product of C_3AH_6 in aqueous media. Since an LDH phase is not discernible after 2 h of contact time (Fig. 5a), its appearance after 1 day is likely to be due to the longer reaction time and thus suggests this phase to be C_4AH_{11}. (Although the presence of Ca_4AcH_{11} cannot be excluded, our observations suggest the Bayer phase to be less prone to carbonation and subsequent carbonate LDH formation than cement C_3AH_6.)

Conversely, the peak at 11.9° shifts to 11.4° in 1 M NaCl (Fig. 7b, inset), indicating that the spacing between the layer increases from 0.74 nm to 0.78 nm. (The estimated uncertainty of the device is ±0.2° 2θ.) The latter is in very good agreement with the basal spacing of an as-prepared chloride-hydrocalumite reported earlier [81]. This noticeable change strongly suggests an ion exchange process between interlayer OH^- and bulk Cl^- ions in concentrated NaCl solution, yielding the formation of chloride-hydrocalumite. Also, the small difference between Bragg spacings is consistent with the similar sizes of the two ions.

Upon addition of HCl, the reflection patterns change markedly: the LDH phase (LDH1 in Fig. 7) becomes the dominant one over C_3AH_6 already at 1 equiv. HCl, and katoite disappears completely at 2 equiv. HCl in both media, accompanied by a decrease in pH of ~1.3 (H_2O) and ~ 1 (1 M NaCl), respectively. That is, reaction of C_3AH_6 with HCl results in the formation of LDH; therefore, this transformation depends heavily on the solution pH. The thus forming LDH persists even up to 5 equiv. acid (not shown), where the pH is approximately 10.2 in both media. Further, the reflection at 11.9° (in H_2O) shifts to 11.4° (Fig. 7a), again suggesting the replacement of OH^- ions by Cl^- ions in the interlayer space of the LDH upon neutralization with HCl. Such shift cannot be detected in 1 M NaCl (Fig. 7b), since the minor hydrocalumite fraction present in C_3AH_6 is already of chloride-type. Furthermore, a third, largely amorphous phase appears in both series, which nevertheless exhibits two distinctive peaks at ~18.6° and ~ 20.4°, which we can assign to the (002) and (110) reflections of gibbsite or bayerite AH_3 (PDF #70–2038, #83–2256 [65]). In conclusion, these transformations suggest the following reaction to take place:

$$2Ca_3Al_2(OH)_{12}(s) + 6HCl(aq) + 4H_2O(aq) \rightarrow Ca_4\left[Al(OH)_6\right]_2Cl_2 \bullet 4H_2O(s) + 2CaCl_2(aq) + 2Al(OH)_3(s) \quad (5)$$

The formation of AH_3 is preferred over aluminate, as shown by the very low values $[Al(III)]_T$ obtained via gravimetry; see Fig. S7, SI.

At 6 equivalents added HCl, only amorphous AH_3 is present as the solubility-controlling solid phase as suggested by Eq. (4). We indeed observed the formation of a gel-like mixture during the addition of acid to the suspension. We note that this phase is not necessarily identical to the one forming during titrations, where smaller aliquots of HCl were added sequentially applying a waiting time of 2 h at each step, hence there formation of an AH_3 phase with higher degree of crystallinity is more likely.

Entering the acidic pH regime, we detect very small peaks at ~11.3° in H_2O (Fig. 7a), suggesting a minor fraction of LDH to be formed. The presence of such hydrocalumite-type material is much more pronounced in the case of 1 M NaCl (Fig. 7b, indicated as LDH2), which however is different from the one forming in the alkaline range. For instance, only a single, broad reflection is discernible at 22.6° instead of the two sharp ones at 22.8° and 23.5°. Nevertheless, the LDH structure is obvious as reflections associated with basal spacings at 22.6° and 34.7°, corresponding to diffractions from the second and third layers, respectively. Possibly, this is a transformation reaction between the LDH1 and LDH2: as LDH1 dissolves, a fraction of the ions reprecipitate as LDH2. Certainly, the presence of this phase in an acidic medium is surprising, and its identification would require further studies, which is however outside the scope of this work. In addition, AH_3 is present in both media in a more crystalline form as compared to the one at 6 equiv. acid.

3.2.4. *Identification of the LDH phase forming in alkaline medium*

We now focus on the qualitative and quantitative analysis of the hydrocalumite phase forming in the pH range of 10.2–11.8. Since the intercalation of the Cl^- ion is the most likely in both media, we compare the XRD patterns taken at 2. equiv. HCl, where this solid is the dominant

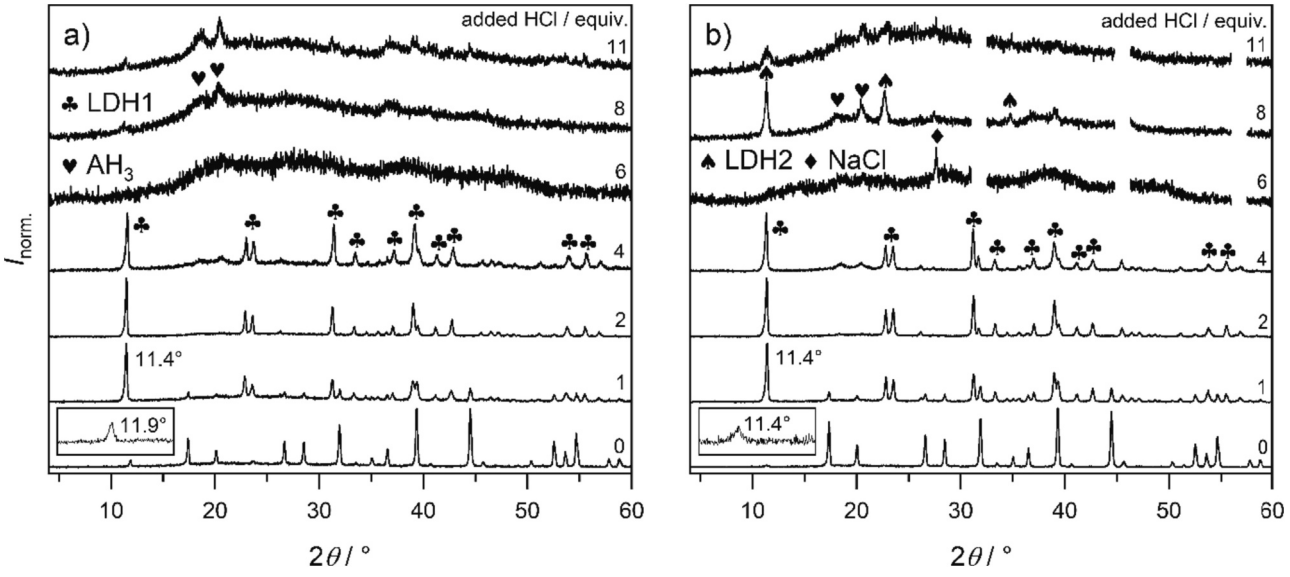

Fig. 7. Traces of powder XRD of Bayer C_3AH_6 after adding different equivalents of HCl to suspensions of 100 g L^{-1} (stirred for 1 day) in a) H_2O or b) 1 M NaCl. Symbols show new phases forming upon neutralization, where $AH_3 = 2Al(OH)_3$ and LDH = layered double hydroxide. In panel b), for residual NaCl, only the (111) reflections are shown for better visibility. In both panels, the inset shows a zoomed region of 10–14° 2θ. Measured data were normalized such that the highest value is unity.

one, to that of Friedel's salt, $Ca_4ACl_2H_{10}$ (PDF #31–0245 [65]). The diffractograms in Fig. 8 demonstrate that our LDH is identical to $Ca_4ACl_2H_{10}$, with the corresponding basal spacings (Table 2) being in excellent agreement with literature data [81]. To support this finding, we performed EDS measurement on several batch samples for both H_2O and 1 M NaCl. The respective Ca:Al and Ca:Cl molar ratios are listed in Table 2. Already at 1 equiv. HCl, the Ca:Cl ratio is very close to 2:1 for both media, which confirms the solid being Friedel's salt. On the other hand, the Ca:Al ratio is lower than 2:1, indicating the presence of excess AH_3 arising predominantly from the reaction between C_3AH_6 and HCl; see Eq. (5).

To quantify the exact amount of water, n, of the $Ca_4ACl_2H_n$ phases forming at 2 equiv. HCl, we carried out TG-MS measurements which report not only on the mass losses, but also on the nature of molecules forming in the respective decomposition step. The TG curves show four distinct losses for Bayer C_3AH_6 in H_2O (Fig. 9a) and 1 M NaCl (Fig. 9b). Based on literature findings, the first decomposition process corresponds to the release of physisorbed and interlayer water molecules, whereas the second and third are attributable to the water forming from Ca^{2+} and Al^{3+}-bound OH^--ions, respectively [49,82–85]. However, XRD patterns show the presence of AH_3 in our samples, which dehydrates also in the temperature range of 250–300 °C [21,46,85]. All these water losses are strongly supported by the peaks appearing at $m/z = 18$ in the mass spectra (insets in Fig. 9). Conversely, the fourth loss appears at 690–730 °C is CO_2, indicative of calcite forming in situ [82], which in turn signals the presence of Ca_4AcH_{11} formed probably during filtration of the suspensions. (C_3AH_6 being the source of CO_2 can be ruled out as we observe no significant carbonate peak for katoites, see Fig. 3.)

As there are three phases in these solids ($Ca_4ACl_2H_n$, Ca_4AcH_{11}, and AH_3), calculation of n is not trivial, therefore we make the following assumptions: 1) based on the ideal Ca:Cl = 2:1 ratio by EDS and the small carbonate loss found by TG-MS, we neglect its contribution, 2) we set the $Ca_4ACl_2H_n$: AH_3 molar ratio to be 1:2 as suggested by Eq. (5), and (3) we assume that the total dehydration process is completed up to 630 °C, as deduced from the MS spectra. Accordingly, we find n to be 9.25 for H_2O and 8.94 in 1 M NaCl, respectively, which is less than the expected theoretical value of 10. Previously, almost the same discrepancy has been found between the experimental and theoretical loss for neat Friedel's salt, attributed to water loss during the drying procedure [49], which is also possible in our case.

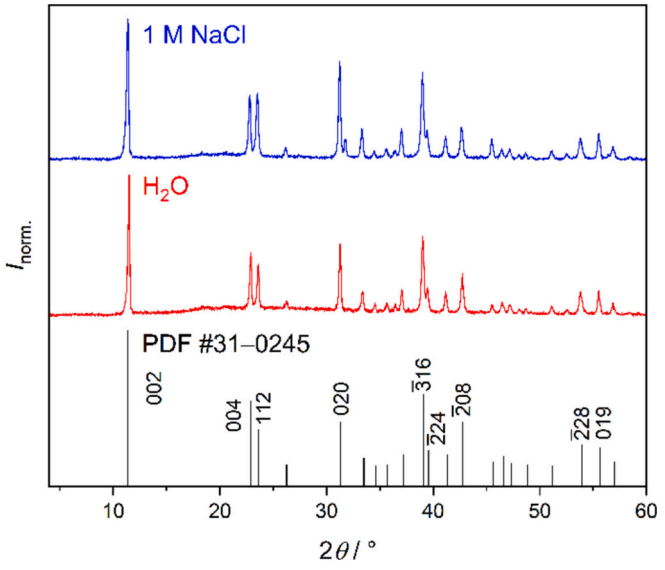

Fig. 8. Traces of powder XRD of Bayer C_3AH_6 after adding 2 equivalents of HCl to suspensions of 100 g L^{-1} (stirred for 1 day) in H_2O (red) or 1 M NaCl (blue). The black diffractogram stands for literature reference of chloride-hydrocalumite or Friedel's salt, $Ca_4AlCl_2H_{10}$ (PDF #31–0245 [65]); shown are also the *hkl* indices of the most intense reflections. Measured data were normalized such that the highest value is unity. (For interpretation of the references to colour in this figure legend, the reader is referred to the web version of this article.)

Table 2
Ca:Al as well as Ca:Cl molar ratios of Bayer C_3AH_6 at different added equivalents of HCl, obtained by EDS analysis. Also shown is the composition at 2. equiv. HCl, determined from EDS and TG-MS analyses.

Medium	Added HCl / equiv.	Composition	Basal spacing / nm	Ca:Al	Ca:Cl
H_2O	1			1.3	2.2
	2	$Ca_4[Al(OH)_6]_2Cl_2 \bullet 3.25H_2O$	0.77	± 0.1 1.4	± 0.2 2.2
				± 0.2	± 0.2
1 M NaCl	1			1.7	2.0
	2	$Ca_4[Al(OH)_6]_2Cl_2 \bullet 2.94H_2O$	0.78	± 0.3 1.8	± 0.6 2.1
				± 0.1	± 0.1

3.3. The equilibrium reaction between katoite and Friedel's salt

Based on time-dependent and close-to-equilibrium powder X-ray diffractograms augmented by potentiometric titrations, TG-MS and EDS measurements, we find C_3AH_6 to spontaneously transform to Friedel's salt (and AH_3) upon addition of HCl. 2 equivalents of added acid gives rise to complete transformation of one solid phase to the other. This seems to contradict Eq. (5), which suggests 3 equiv. HCl per C_3AH_6 to be needed. Strictly speaking, the equation holds true only if both solids are insoluble. Consequently, Eq. (5) is more likely an equilibrium process, where the actual concentrations are described by an equilibrium constant. This equilibrium emerges from combining the dissolution reaction of C_3AH_6 (Eqs. (1) and (2)) and that of $C_4ACl_2H_{10}$ (Eqs. (6) and (7)):

$$Ca_4\left[Al(OH)_6\right]_2Cl_2 \bullet 4H_2O(s) \rightleftharpoons 4Ca^{2+}(aq) + 2Al(OH)_4{}^-(aq) + 2Cl^-(aq) + 4OH^-(aq) + 4H_2O(aq) \quad (6)$$

$$K_{sp}(C_4ACl_2H_{10}) = \left\{Ca^{2+}\right\}^4\left\{Al(OH)_4{}^-\right\}^2\left\{Cl^-\right\}^2\left\{OH^-\right\}^4 \quad (7)$$

$$Ca_3Al_2(OH)_{12}(s) + Cl^-(aq) + 2H_2O(aq) \rightleftharpoons \frac{1}{2}Ca_4\left[Al(OH)_6\right]_2Cl_2 \bullet 4H_2O(s) + Ca^{2+}(aq) + Al(OH)_4{}^-(aq) + 2OH^-(aq) \quad (8)$$

where the corresponding equilibrium constant, K, reads as:

$$K = \left\{Ca^{2+}\right\}\left\{Al(OH)_4{}^-\right\}\left\{OH^-\right\}^2/\left\{Cl^-\right\} \quad (9)$$

Based on literature data for the two solubility products [15], $\log K = \log K_{sp}(C_3AH_6) - 0.5\log K_{sp}(C_4ACl_2H_{10}) = -6.87$. This negative value explains the general observation of C_3AH_6 being the thermodynamically more stable phase compared to LDH and other AFm compounds [35,46,49].

Moreover, it is instructive to assess the effect of excess H^+ ions upon addition of HCl:

$$Ca_3Al_2(OH)_{12}(s) + 2H^+(aq) + Cl^-(aq) \rightleftharpoons \frac{1}{2}Ca_4\left[Al(OH)_6\right]_2Cl_2 \bullet 4H_2O(s) + Ca^{2+}(aq) + Al(OH)_4{}^-(aq) \quad (10)$$

$$K' = \left\{Ca^{2+}\right\}\left\{Al(OH)_4{}^-\right\}/\left(\left\{Cl^-\right\}\left\{H^+\right\}^2\right) \quad (11)$$

Accordingly, $\log K' = \log K + 2pK_w = 21.14$, where $pK_w = 14$ is the negative logarithm of the water ionic product. (Given that all the above constants correspond to infinite dilution, we assumed the activity of

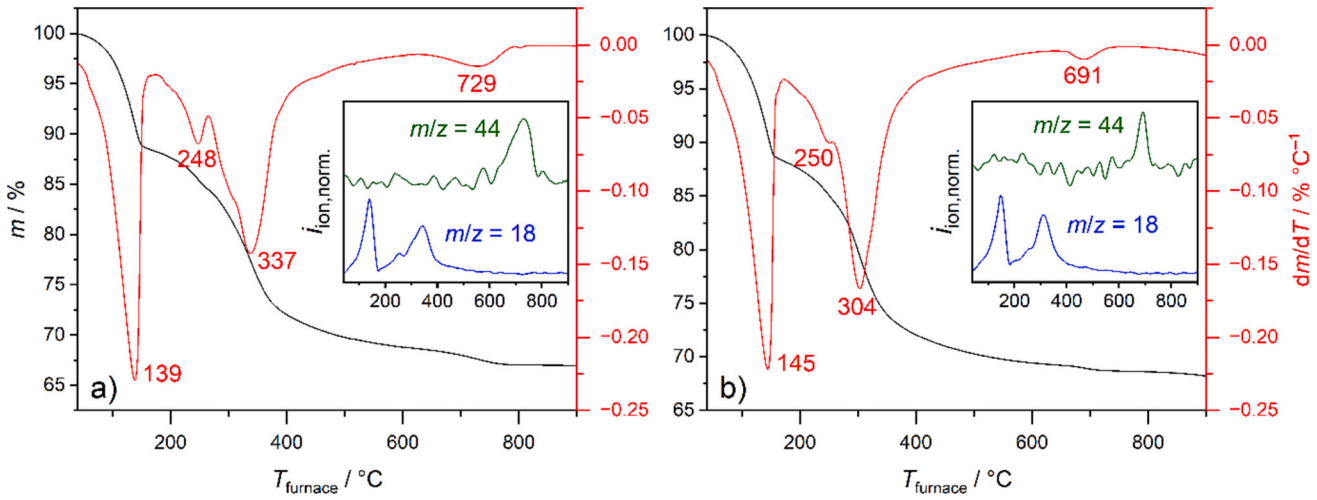

Fig. 9. Thermogravimetric analysis of solids obtained after addition of 2 equivalents of HCl to suspensions of Bayer C_3AH_6 of 100 g L^{-1} (stirred for 1 day) in a) H_2O or b) 1 M NaCl. The left axis corresponds to the mass loss upon heating (black), while the right axis shows its derivative (red). Also shown are the characteristic losses, each corresponding to an inflection point on the TG curve. In both panels, the insets show the corresponding intensities of decomposition products H_2O ($m/z = 18$, blue) and CO_2 ($m/z = 44$, green) as obtained from TG-MS. Measured ion current intensities were normalized such that the highest value is unity. (For interpretation of the references to colour in this figure legend, the reader is referred to the web version of this article.)

water, a_w, to be 1 in the expressions.) In conclusion, upon decreasing the pH (by adding HCl), the transformation becomes highly favorable. In other words, addition of HCl drives the reaction to the right, as follows from Le Chatelier's principle, giving rise to the disappearance of katoite already at 2 equiv. HCl. That is, the range between 0 and 2 equiv. HCl, corresponding to ca. 11 < pH < 12, is a region where C_3AH_6 and $C_4ACl_2H_{10}$ (as well as AH_3) are likely to coexist, which is reinforced by previous findings regarding aqueous suspensions aged for 17 months (albeit employing excess calcium(II)) [49]. In this respect, further studies with longer time-window may be useful to pinpoint the pH range of coexistence.

On the other hand, the principle suggests the same effect (although not of the same magnitude) when adding NaCl. Thus, the apparent slowdown of the formation of Friedel's salt in 1 M NaCl, demonstrated by Fig. 5, signals that other kinetic factors might be at play [73–75]. Nevertheless, this slowdown is consistent with the differences observed between the titration curves in H_2O and 1 M NaCl; see Fig. 6 (green vs. blue full squares). That is, having most but not all of the added acid consumed by C_3AH_6, smaller than the equilibrium amount of $C_4ACl_2H_{10}$ forms in 1 M NaCl, resulting in a lower pH as compared to H_2O medium. In the second step, residual C_3AH_6 continiues to slowly transform to $C_4ACl_2H_{10}$ to attain equilibrium, which increases the pH at the same time, as described by Eq. (8).

To further support the equilibrium described by Eqs. (8) and (9), we conducted an experiment, in which we first added 2 equiv. HCl to a 100 g L^{-1} suspension of Bayer C_3AH_6 in H_2O. Here, only $C_4ACl_2H_{10}$ and amorphous AH_3 are detectable; see Figs. 8 and 10 (the corresponding pH is 11.0). After 1 day, we added 2 equiv. NaOH to recover the initial pH and measured the diffractogram of the solid after another day. Unexpectedly, we find the pH to increase to 13.3, which is much higher than the pH of an initial C_3AH_6 suspension (12.3). The powder diffractogram of the solid phase shows the major phase to be still $C_4ACl_2H_{10}$, and the two most intensive reflections of C_3AH_6 are also discernible (inset in Fig. 10). This demonstrates that the transformation of katoite to Friedel's salt is reversible. However, despite the former being the thermodynamically stable phase at pH = 13.3, it is a minor phase indicating that the reverse process, i.e. $C_4ACl_2H_{10} \rightarrow C_3AH_6$, is kinetically hindered, which in turn explains why most of the added NaOH was not consumed (Eq. (8)).

The proposed reaction scheme between C_3AH_6, $C_4ACl_2H_{10}$ and AH_3 may have important implications for the hydration of C_3A. In the absence of gypsum, C_3A is known to transform into LDH phases, e.g. C_2AH_8 and C_4AH_{13}, with $Al(OH)_4^-$ and OH^- ions, respectively, being intercalated between the layers [4,7,38,41,42,48].

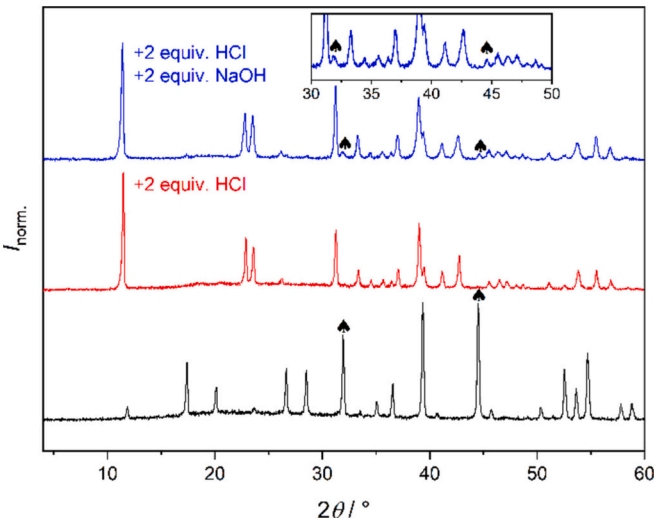

Fig. 10. Traces of powder XRD of Bayer C_3AH_6 suspensions of 100 g L^{-1} in H_2O, stirred for 1 day (black), stirred for 1 day after adding 2 equivalents of HCl (red) and stirred for another day after adding further 2 equivalents of NaOH (blue). Black symbols show the (420) and (611) reflections of C_3AH_6 (PDF #24–0217 [65]) which appear as small peaks after the addition of 2 equiv. NaOH, due to its reformation. Measured data were normalized such that the highest value is unity. (For interpretation of the references to colour in this figure legend, the reader is referred to the web version of this article.)

$$Ca_3Al_2O_{12}(s) + 21H_2O(aq) \rightarrow Ca_2\left[Al(OH)_6\right]Al(OH)_4 \bullet 3H_2O(s) + Ca_4\left[Al(OH)_6\right]_2(OH)_2 \bullet 6H_2O(s) \rightarrow 2Ca_3Al_2(OH)_{12}(s) + 9H_2O(aq) \quad (11)$$

To estimate the net pH change accompanying this reaction, it is useful to look at the thermodynamic solubility products of C_3A [22] and C_3AH_6 [15]. Accordingly, the pH controlled by the dissolution of the respective solid is ~8.8 (C_3A) and ~ 11.8 (C_3AH_6), respectively, at room temperature. Based on the pH-dependent equilibrium between C_3AH_6,

$C_4ACl_2H_{10}$, such reversible transformation is possible between C_3AH_6, C_2AH_8 and C_4AH_{13}, too. Therefore, at the initial stages of hydration, where the pH is rather low, even if C_3AH_6 incidentally forms, it readily transforms into the LDH phases. Conversely, approaching thermodynamic equilibrium at later times, the steady increase in pH promotes the formation of C_3AH_6 which will eventually be the thermodynamically stable phase.

4. Conclusions

In this contribution, we synthesized and compared tricalcium aluminate hexahydrate or katoite, C_3AH_6, via the conventional synthesis based on the hydration of C_3A in cementitious materials (cement C_3AH_6); as well as via a high-temperature, alkaline digestion method under the conditions of the Bayer process (Bayer C_3AH_6). Comparison of the structural, textural properties, and compositions of the thus obtained products shows that they are largely similar.

Further, we studied the dissolution and acid neutralization behavior of the two katoites using H_2O and 1 M NaCl, respectively, as dispersion medium. We found that upon reacting with HCl, both cement and Bayer C_3AH_6 transform to Friedel's salt, $C_4ACl_2H_{10}$, a layered double hydroxide with Cl^- ions intercalated between the layers. In the alkaline region, the neutralization slows down in 1 M NaCl, which is possibly due to the blocking effect of Cl^- ions of active dissolution sites of katoite particles, as found previously in the presence of SO_4^{2-} ions. At pH ≈ 7, the only solid phase is amorphous AH_3. Decreasing the pH further, addition of 0.3–1 M NaCl markedly accelerates the dissolution of AH_3, which is the opposite effect of what has been reported earlier for in very dilute salt solutions.

In equilibrium, we find that the addition of 2 equiv. HCl gives rise to complete transformation of C_3AH_6 to $C_4ACl_2H_{10}$, regardless of the dispersion medium. That is, excess protons render this reaction highly favorable, which can be elucidated by an equilibrium between the two calcium aluminate phases and AH_3. Moreover, addition of NaOH to the thus obtained suspension provides evidence for the reversibility of the process. However, the $C_4ACl_2H_{10} \rightarrow C_3AH_6$ reaction is kinetically hindered, indicating the critical role of chloride ions in stabilizing the structure of LDH.

Overall, we find these phases to coexist in the pH range of 11–12, and the actual phase composition is intimately related to the solution pH. This finding may have important implications for other LDH phases with different intercalated ions as well; most importantly, C_2AH_8 and C_4AH_{13}, whose formation precedes that of C_3AH_6 during the hydration of C_3A.

CRediT authorship contribution statement

Eszter Kása: Data curation, Investigation, Methodology, Validation, Visualization, Writing – original draft, Writing – review & editing. **Yvette Szabó:** Data curation, Investigation, Methodology, Writing – review & editing. **Márton Szabados:** Formal analysis, Methodology, Supervision, Writing – review & editing. **Ákos Kukovecz:** Methodology, Resources, Writing – review & editing. **Zoltán Kónya:** Methodology, Resources, Writing – review & editing. **Pál Sipos:** Conceptualization, Funding acquisition, Methodology, Project administration, Supervision, Writing – review & editing. **Bence Kutus:** Conceptualization, Data curation, Formal analysis, Investigation, Methodology, Project administration, Supervision, Validation, Visualization, Writing – original draft, Writing – review & editing.

Declaration of competing interest

The authors declare that they have no known competing financial interests or personal relationships that could have appeared to influence the work reported in this paper.

Data availability

Data will be made available on request.

Acknowledgements

The authors are grateful to I. Halasiné-Varga for her technical assistance, to K. Baán (University of Szeged) for the BET, to Sz. Ziegenheim and Zs. Kása for their assistance in the ICP-MS measurements, and to Dr. G. Szalontai (Pannon University) for the MAS NMR measurements. E. Kása thanks for the financial support to the ÚNKP–21–3-SZTE-451 scholarship of the New National Excellence Program by the Ministry of Culture and Innovation and the National Research, Development and Innovation Office. M. Szabados and B. Kutus gratefully acknowledge the support of Bolyai Janos Research Fellowship (BO/00246/21/7; BO/00551/23/7) of the Hungarian Academy of Sciences and M. Szabados acknowledges the ÚNKP-22-5-SZTE-589 New National Excellence Program of the Ministry for the Innovation and Technology from the National Research, Development and Innovation Office.

Appendix A. Supplementary data

Supplementary data to this article can be found online at https://doi.org/10.1016/j.cemconres.2023.107414.

References

[1] Statista Inc., Cement production worldwide from 1995 to 2021. https://www.statista.com/statistics/219343/cement-production-worldwide/, 2022 (accessed 2 February 2023).
[2] J.D. Birchall, A.J. Howard, J.E. Bailey, On the hydration of Portland cement, Proc. R. Soc. London A 360 (1978) 445–453.
[3] X. Cong, R.J. Kirkpatrick, Hydration of calcium sulfoaluminate cements: a solid-state ^{27}Al NMR study, J. Am. Ceram. Soc. 76 (1993) 409–416.
[4] H.F.W. Taylor, Cement Chemistry, second ed., Thomas Telford, London, UK, 1997.
[5] B. Lothenbach, F. Winnefeld, Thermodynamic modelling of the hydration of Portland cement, Cem. Concr. Res. 36 (2006) 209–226.
[6] F. Winnefeld, B. Lothenbach, Hydration of calcium sulfoaluminate cements – experimental findings and thermodynamic modelling, Cem. Concr. Res. 40 (2010) 1239–1247.
[7] L.G. Baquerizo, T. Matschei, K.L. Scrivener, M. Saeidpour, L. Wadsö, Hydration states of AFm cement phases, Cem. Concr. Res. 73 (2015) 143–157.
[8] H.M. Saleh, S.B. Eskander, Innovative cement-based materials for environmental protection and restoration, in: P. Samui, N.R. Iyer, D. Kim, S. Chaudhary (Eds.), New Materials in Civil Engineering, Butterworth-Heinemann, Oxford, UK, 2020, pp. 513–641.
[9] D.G. Bennett, D. Read, M. Atkins, F.P. Glasser, A thermodynamic model for blended cements. II: cement hydrate phases; thermodynamic values and modelling studies, J. Nucl. Mater. 190 (1992) 315–325.
[10] E.J. Reardon, Problems and approaches to the prediction of the chemical composition in cement/water sytems, Waste Manag. 12 (1992) 211–239.
[11] V.A. Sinitsyn, D.A. Kulik, M.S. Khodorivsky, I.K. Karpov, Mater. Res. Soc. Symp. Proc. 506 (1997) 953–960.
[12] T. Matschei, B. Lothenbach, F.P. Glasser, Thermodynamic properties of Portland cement hydrates in the system $CaO–Al_2O_3–SiO_2–CaSO_4–CaCO_3–H_2O$, Cem. Concr. Res. 37 (2007) 1379–1410.
[13] Ph. Blanc, X. Bourbon, A. Lassin, E.C. Gaucher, Chemical model for cement-based materials: temperature dependence of thermodynamic functions for nanocrystalline and crystalline C-S-H phases, Cem. Concr. Res. 40 (2010) 851–866.
[14] Ph. Blanc, X. Bourbon, A. Lassin, E.C. Gaucher, Chemical model for cement-based materials: thermodynamics data assessment for phases other than C-S-H, Cem. Concr. Res. 40 (2010) 1360–1374.
[15] B. Lothenbach, D.A. Kulik, T. Matschei, M. Balonis, L. Baquerizo, B. Dilnesa, G. D. Miron, R.J. Myers, Cemdata18: a chemical thermodynamic database for hydrated Portland cements and alkali-activated materials, Cem. Concr. Res. 115 (2019) 472–506.
[16] B. Lothenbach, M. Zajac, Application of thermodynamic modelling to hydrated cements, Cem. Concr. Res. 123 (2019), 105799.
[17] K.J.D. Mackenzie, R.K. Banerjee, Formation kinetics of Portland cement clinker phases. 1–Tricalcium aluminate, Trans. J. Brit. Ceram. Soc. 77 (1978) 88–92.
[18] G. Kakali, S. Tsivilis, E. Aggeli, M. Bati, Hydration products of C_3A, C_3S and Portland cement in the presence of $CaCO_3$, Cem. Concr. Res. 30 (2000) 1073–1077.
[19] H.J.H. Brouwers, R.J. van Erik, Alkali concentrations of pore solution in hydrating OPC, Cem. Concr. Res. 33 (2003) 191–196.
[20] M.C.G. Juenger, F. Winnefeld, J.L. Provis, J.H. Ideker, Advances in alternative cementitious binders, Cem. Concr. Res. 41 (2011) 1232–1243.

[21] S. Barzgar, Y. Yan, M. Tarik, J. Skibsted, C. Ludwig, B. Lothenbach, A long-term study on structural changes in calcium aluminate silicate hydrates, Mater. Struct. 55 (2022) 243.

[22] S. Ye, P. Feng, J. Lu, L. Zhao, Q. Liu, Q. Zhang, J. Liu, J.W. Bullard, Solubility of tricalcium aluminate from 10 °C to 40 °C, Cem. Concr. Res. 162 (2022), 106989.

[23] M.C. Martín-Sedeno, A.J.M. Cuberos, Á.G. De la Torre, G. Álvarez-Pinazo, L. M. Ordónez, M. Gateshki, M.A.G. Aranda, Aluminum-rich belite sulfoaluminate cements: clinkering and early age hydration, Cem. Concr. Res. 40 (2010) 359–369.

[24] C. Si, A. Fernández-Jiménez, A. Palomo, New cements for the 21st century: the pursuit of an alternative to Portland cement, Cem. Concr. Res. 41 (2011) 750–763.

[25] D. Gastaldi, G. Paul, L. Marchese, S. Irico, E. Boccaleri, S. Mutke, L. Buzzi, F. Canonico, Hydration products in sulfoaluminate cements: evaluation of amorphous phases by XRD/solid-state NMR, Cem. Concr. Res. 90 (2016) 162–173.

[26] L.U.D. Tambara Júnior, J.C. Rocha, M. Cheriaf, P. Padilla-Encinas, A. Fernández-Jiménez, A. Palomo, Effect of alkaline salts on calcium sulfoaluminate cement hydration, Molecules 26 (2021) 1938.

[27] F. Bertola, D. Gastaldi, S. Irico, G. Paul, F. Canonico, Influence of the amount of calcium sulfate on physical/mineralogical properties and carbonation resistance of CSA-based cements, Cem. Concr. Res. 151 (2022), 106634.

[28] K. Quillin, Performance of belite-sulfoaluminate cements, Cem. Concr. Res. 31 (2001) 1341–1349.

[29] E. Gartner, Industrially interesting approaches to "low-CO_2" cements, Cem. Concr. Res. 34 (2004) 1489–1498.

[30] M. Singh, S.N. Upadhayay, P.M. Prasad, Preparation of special cements from red mud, Waste Manag. 16 (1996) 665–670.

[31] S. Galluccio, T. Beirau, H. Pöllmann, Maximization of the reuse of industrial residues for the production of eco-friendly CSA-belite clinker, Constr. Build. Mater. 208 (2019) 250–257.

[32] O. Canbek, S. Shakouri, S.T. Erdoğan, Laboratory production of calcium sulfoaluminate cements with high industrial waste content, Cem. Concr. Compos. 106 (2020), 103475.

[33] Y. Gao, Z. Li, J. Zhang, Q. Zhang, Y. Wang, Synergistic use of industrial solid wastes to prepare belite-rich sulphoaluminate cement and its feasibility use in repairing materials, Constr. Build. Mater. 264 (2020) 12021.

[34] S. Wu, X. Yao, C. Ren, Y. Yao, C. Zhang, C. Wu, W. Wang, Effect of iron on the preparation of iron-rich calcium sulfoaluminate cement using gypsum as the sole calcium oxide source and its incorporation into mineral phases, Constr. Build. Mater. 290 (2021), 123214.

[35] S.P. Rosenberg, D.J. Wilson, C.A. Heath, Some aspects of calcium chemistry in the Bayer process, in: D. Donaldson, B. Raahuge (Eds.), Essential Readings in Light Metals vol. 1, Alumina and Bauxite, John Wiley & Sons, Hoboken, NJ, U.S, 2016, pp. 210–216.

[36] J. Vogrin, H. Hodge, T. Santini, H. Peng, J. Vaughan, Quantitative X-ray diffraction study into bauxite residue mineralogical phases, in: C. Chesonis (Ed.), Light Metals 2019, The Minerals, Metals & Materials Society, Pittsburgh, PA, U.S., 2019, pp. 93–99.

[37] H. N. Stein, The reaction of 3 CaO,Al_2O_3 with water in the presence of $CaSO_4,2H_2O$, J. Appl. Chem. 13 (1963) 228–232.

[38] E. Breval, C_3A hydration, Cem. Concr. Res. 6 (1976) 129–138.

[39] M. Collepardi, G. Baldini, M. Pauri, M. Corradi, Retardation of tricalcium aluminate hydration by calcium sulfate, J. Am. Chem. Soc. 62 (1979) 33–35.

[40] T. Wang, P. Zhang, D. Wu, M. Sun, Y. Deng, R.L. Frost, Effective removal of zinc (II) from aqueous solutions by tricalcium aluminate (C_3A), J. Colloid Interface Sci. 443 (2015) 65–71.

[41] S. Joseph, J. Skibsted, Ö. Cicer, A quantitative study of the C_3A hydration, Cem. Concr. Res. 115 (2019) 145–159.

[42] T. Hirsch, T. Matschei, D. Stephan, The hydration of tricalcium aluminate ($Ca_3Al_2O_6$) in Portland-cement-related systems: a review, Cem. Concr. Res. 168 (2023), 107150.

[43] F.P. Glasser, M.B. Marinho, Early stages of the hydration of tricalcium aluminate and its sodium-containing solid solutions, Proc. Br. Ceram. Soc. 35 (1984) 221–236.

[44] K.L. Scrivener, P.L. Pratt, Microstructural studies of the hydration of C_3A and C_4AF independently and in cement phase, Proc. Br. Ceram. Soc. 35 (1984) 207–219.

[45] L. Black, C. Breen, J. Yarwood, C.-S. Deng, J. Phipps, G. Maitland, Hydration of tricalcium aluminate (C_3A) in the presence and absence of gypsum–studied by Raman spectroscopy and X-ray diffraction, J. Mater. Chem. 16 (2006) 1263–1272.

[46] B. Lothenbach, L. Pelletier-Chaignat, F. Winnefeld, Stability in the system $CaO-Al_2O_3-H_2O$, Cem. Concr. Res. 42 (2012) 1621–1634.

[47] S. Khaitan, D.A. Dzombak, G.V. Lowry, Chemistry of the acid neutralization capacity of bauxite residue, Environ. Eng. Sci. 26 (2009) 873–881.

[48] Gy. Balázs, J. Csizmadia, K. Kovács, Chloride ion binding ability of calcium-aluminate, -ferrite and and -silicate phases, Period. Polytech. Civ. Eng. 41 (1997) 147–168.

[49] U. A. Birnin-Yauri, F. P. Glasser, Friedel's salt, $Ca_2Al(OH)_6(Cl,OH)\bullet 2H_2O$: its solid solutions and their role in chloride binding, Cem. Concr. Res. 28 (1998) 1713–1723.

[50] G. Paul, E. Boccaleri, L. Buzzi, F. Canonico, D: Gastaldi, Friedel's salt formation in sulfoaluminate cements: a combined XRD and ^{27}Al MAS NMR study, Cem. Concr. Res. 67 (2015) 93–102.

[51] C. Shi, X. Hu, X. Wang, Z. Wu, G. de Schutter, Effects of chloride ion binding on microstructure of cement pastes, J. Mater. Civ. Eng. 29 (2017), 04016183.

[52] Y. Jo, I. Androniuk, N. Çevirim-Papioannou, B. de Blochouse, M. Altmaier, X. Gaona, Uptake of chloride and iso-saccharinic acid by cement: sorption and molecular dynamics studies on HCP (CEM I) and C-S-H phases, Cem. Concr. Res. 157 (2022), 106831.

[53] X. Ming, Y. Li, Q. Liu, M. Wang, Y. Cai, B. Chen, Z. Li, Chloride binding behaviors and early age hydration of tricalcium aluminate in chloride-containing solutions, Cem. Concr. Compos. 137 (2023), 104928.

[54] A. Gácsi, B. Kutus, Z. Kónya, Á. Kukovecz, I. Pálinkó, P. Sipos, Estimation of the solubility product of hydrocalumite–hydroxide, a layered double hydroxide with the formula of $[Ca_2Al(OH)_6]OH\bullet nH_2O$, J. Phys. Chem. Solids 98 (2016) 167–173.

[55] S. Gražulis, D. Chateigner, R.T. Downs, A.F.T. Yokochi, M. Quirós, L. Lutterotti, E. Mankova, J. Butkus, P. Moeck, A. Le Bail, Cristallography open database – an open-access collection of crystal structures, J. Appl. Crystallogr. 42 (2009) 726–729.

[56] D. Zagorac, H. Müller, S. Ruehl, J. Zagorac, S. Rehme, Recent developments in the inorganic crystal structure database: theoretical crystal structure data and related features, J. Appl. Crystallogr. 52 (2019) 918–925.

[57] U. Berner, A Thermodynamic Description of the Evolution of Pore Water Chemistry and Uranium Speciation during Degradation of Cement, Report No. 62,, Paul Scherrer Institute, Villigen, Switzerland, 1990.

[58] S. Yousuf, P. Shafigh, Z. Ibrahim, The pH of cement-based materials: a review, J. Wuhan. Univ. Technol. Mater. Sci. Ed. 35 (2020) 908–924.

[59] B.Z. Dilnesa, B. Lothenbach, G. Renaudin, A. Wichser, D. Kulik, Synthesis and characterization of hydrogarnet $Ca_3(Al_xFe_{1-x})_2(SiO_4)_y(OH)_{4(3-y)}$, Cem. Concr. Res. 59 (2014) 96–111.

[60] E. Litwinek, D. Madej, Structure, microstructure and thermal stability characterizations of C_3AH_6 synthesized from different precursors through hydration, J. Therm. Anal. Calorim. 139 (2019) 1693–1706.

[61] R. Salimi, J. Vaughan, H. Peng, Solubility of tricalcium aluminate in synthetic spent Bayer liquor, Ind. Eng. Chem. Res. 53 (2014) 17499–17505.

[62] P. Sipos, P.M. May, G.T. Hefter, Carbonate removal from concentrated hydroxide solutions, Analyst 125 (2005) 955–958.

[63] P. Sipos, G. Hefter, P.M. May, A hydrogen electrode study of concentrated alkaline aluminate solutions, Aust. J. Chem. 51 (1998) 445–453.

[64] E. Kása, M. Szabados, K. Baán, Z. Kónya, Á. Kukovecz, B. Kutus, I. Pálinkó, P. Sipos, The dissolution kinetics of raw and mechanochemically treated kaolinites in industrial spent liquor – the effect of the physico-chemical properties of the solids, Appl. Clay Sci. 203 (2021), 105994.

[65] S. Gates-Rector, T. Blanton, The powder diffraction file: a quality materials characterization database, Powder Diffract. 34 (2019) 352–360.

[66] C.R. Hubbard, E.H. Evans, D.K. Smith, The reference intensity ratio, I/I_C, for computer simulated powder patterns, J. Appl. Crystallogr. 9 (1976) 169–174.

[67] M. Terato, Y. Suda, T. Saito, T. Saeki, Fundamental study on the estimation method of the specific surface area of hardened cement paste considering calcium aluminate hydrates, Cement Sci. Concr. Technol. 66 (2012) 197–204.

[68] S. Mantellato, M. Palacios, R.J. Flatt, Reliable specific surface area measurements on anhydrous cements, Cem. Concr. Res. 67 (2015) 286–291.

[69] H.-I. Kim, S.K. Lee, Probing the transformation paths from aluminum (oxy) hydroxides (boehmite, bayerite, and gibbsite) to metastable alumina: a view from high-resolution ^{27}Al MAS NMR, Am. Mineral. 106 (2021) 389–403.

[70] C. Ekberg, P.L. Brown, Hydrolysis of Metal Ions, Wiley-VCH, Weinheim, Germany, 2016.

[71] R. Guillaumont, T. Fanghänel, J. Fuger, I. Grenthe, V. Neck, D.A. Palmer, M. H. Rand, Update on the Chemical Thermodynamics of Uranium, Neptunium, Plutonium, Americium and Technetium, Nuclear Energy Agency, Palaiseau, France, 2003.

[72] B. Kutus, C. Dudás, E. Orbán, A. Lupan, A.A.A. Attia, I. Pálinkó, P. Sipos, G: Peintler, Magnesium(II) D-gluconate complexes relevant to radioactive waste disposals: metal-ion-induced ligand deprotonation or ligand-promoted metal-ion hydrolysis? Inorg. Chem. 58 (2019) 6832–6844.

[73] M.E. Tadros, W.Y. Jackson, J. Skalny, Study of the dissolution and electrokinetic behavior of tricalcium aluminate, in: M. Kerker (Ed.), Colloid and Interface Science vol. 4, Hydrosoly and Rheology, Academic Press, London, UK, 1976, pp. 211–223.

[74] H. Minard, S. Garrault, L. Regnaud, A. Nonat, Mechanisms and parameters controlling the tricalcium aluminate reactivity in the presence of gypsum, Cem. Concr. Res. 37 (2007) 1418–1426.

[75] A.S. Brand, S.B. Feldman, P.E. Stutzman, A.V. Ievlev, M. Lorenz, D.C. Pagan, S. Nair, J.M. Gorham, J.W. Bullard, Dissolution and initial hydration behavior of tricalcium aluminate in low activity sulfate solutions, Cem. Concr. Res. 130 (2020), 105989.

[76] M. Altmaier, V. Metz, V. Neck, R. Müller, T. Fanghänel, Solid-liquid equilibria of $Mg(OH)_2(cr)$ and $Mg_2(OH)_3Cl\bullet 4H_2O(cr)$ in the system Mg-Na-H-OH-Cl-H_2O at 25°C, Geochim. Cosmochim. Acta 67 (2003) 3595–3601.

[77] J.L. Mogollón, A. Pérez-Diaz, S. Lo Monaco, The effects of ion identity and ionic strength on the dissolution rate of a gibbsitic bauxite, Geochim. Cosmochim. Acta 64 (2000) 781–795.

[78] J.N. Brönsted, C.E. Teeter Jr., On kinetic salt effect, J. Phys. Chem. 28 (1924) 579–587.

[79] R. Ruiz-Agudo, M. Kowacz, C.V. Putnis, A. Putnis, The role of background electrolytes on the kinetics and mechanism of calcite dissolution, Geochim. Cosmochim. Acta 74 (2010) 1256–1267.

[80] J.Y. Kim, S. Komarneni, R. Parette, F. Cannon, H. Katsuki, Perchlorate uptake by synthetic layered double hydroxides and organo-clay minerals, Appl. Clay Sci. 51 (2011) 158–164.

[81] F. Trolard, Y. Tardy, The stabilities of gibbsite, boehmite, aluminous goethite and aluminous hematites in bauxites, ferricretes and laterites as a function of water activity, temperature and particle size, Geochim. Cosmochim. Acta 51 (1987) 945–957.

[82] A. Jiménez, V. Rives, M.A. Vicente, Thermal study of the hydrocalumite-katoite-calcite system 713 (2022), 179242.

[83] R.O. Grishchenko, A.L. Emelina, P.Y. Makarov, Thermodynamic properties and thermal behavior of Friedel's salt, Thermochim. Acta 570 (2013) 74–79.
[84] L. Vieille, I. Rousselot, F. Leroux, J.-P. Besse, C. Taviot-Guého, Hydrocalumite and its polymer derivatives. 1. Reversible thermal behavior of Friedel's salt: a direct observation by means of high-temperature in stu powder X-ray diffraction, Chem. Mater. 15 (2003) 4361–4368.
[85] X. Du, Y. Wang, X. Su, J. Li, Influences of pH value on the microstructure and phase transformation of aluminum hydroxide, Powder Technol. 192 (2009) 40–46.